Research Article | Vol. 11, No. 1 / 1 January 2020 / Biomedical Optics Express 109
Biomedical Optics EXPRESS

Potential of sub-microsecond laser pulse shaping for controlling microcavitation in selective retinal therapies

PASCAL DELADURANTAYE,[1,2,3,*] SÉBASTIEN MÉTHOT,[1,2] OZZY MERMUT,[3,4] PIERRE GALARNEAU,[3] AND PATRICK J ROCHETTE[1,2,5]

[1]*Axe Médecine Régénératrice, Centre de recherche du CHU de Québec- Université Laval, Hôpital du Saint-Sacrement, Québec, Canada*
[2]*Centre de recherche en Organogénèse Expérimentale de l'Université Laval/LOEX, Université Laval, Québec, Canada*
[3]*Institut National d'Optique (INO), Québec, Canada*
[4]*Department of Physics and Astronomy, York University, Ontario, M3J 1P3, Canada*
[5]*Département d'ophtalmologie, Faculté de Médecine, Université Laval, Québec, Canada*
[*]*pascal.deladurantaye@videotron.ca*

Abstract: Pilot results showing the potential of sub-microsecond laser pulse shaping to optimize thermomechanical confinement in laser-tissue interactions involving microcavitation are presented. Model samples based on aqueous suspensions of retinal melanosomes and eumelanin particles were irradiated at 532 nm with nanosecond laser pulses and picosecond laser pulse trains having differing shapes and durations. The cavitation threshold radiant exposure and the bubble lifetime above the threshold were measured using a pump-probe setup and sub-nanosecond time-resolved imaging. Both quantities were found to strongly depend on the pulse format. These results suggest that sub-microsecond laser pulse shaping could be exploited to optimize precision and control in numerous applications of laser-directed microcavitation, including selective retinal laser treatments.

1. Introduction

Laser-directed microcavitation is a process by which microscopic transient vapor bubbles are generated within a medium, upon heating resulting from the absorption of electromagnetic radiation. This process has important biomedical applications, notably in ophthalmology, where it is employed for selectively damaging target cells and tissues in treatments of retinal diseases such as diabetic retinopathy [1–28]. Laser therapies are targeting the retinal pigment epithelium (RPE), the pigmented layer posterior to the neural retina containing eumelanin-charged melanosomes.

In laser therapies and laser surgery, tissues can be affected both structurally and functionally through different mechanisms, depending on the irradiation conditions and on tissue characteristics. First, heat diffusion around absorbing structures such as melanosomes can lead to thermal denaturation of proteins and/or nucleic acids and eventually causes cell death [29–33]. Secondly, thermo-mechanical effects involving a phase transition can induce transient vapor bubble formation causing mechanical damage to the cells and tissue disruption [29–31,34]. When the laser energy is absorbed at a rate that exceeds the heat diffusion rate in the tissue, heat accumulates in the irradiated volume as it cannot escape via heat conduction, a condition termed *thermal confinement*. Thermal confinement allows for maximizing the temperature in the heated volume and transient bubbles can be created with relatively low absorbed laser energy when the temperature rises above the vaporization temperature of the medium that surrounds the absorbers. This bubble formation mechanism is termed *explosive vaporization*. Heat accumulation also creates thermoelastic stresses due to the thermal expansion of a material. When heat accumulates

#376137 https://doi.org/10.1364/BOE.11.000109
Journal © 2020 Received 28 Aug 2019; revised 8 Nov 2019; accepted 25 Nov 2019; published 6 Dec 2019

Biomedical Optics EXPRESS

faster than the acoustic relaxation rate of the material, a high pressure can build up in the heated volume and thermoelastic stress transients with significant compressive and tensile components can be generated. This condition is called *stress confinement*. Cavitation bubbles can be generated in liquids under stress confinement conditions when the temperature rise produced per laser pulse is sufficient to create a tensile stress wave whose amplitude exceeds the tensile strength of the liquid. This bubble formation mechanism can occur at laser fluences and temperatures that are significantly lower than the ones required for explosive vaporization, and was studied extensively for ultrashort laser pulses [35–37]. In most practical situations, the total volume of tissue affected both thermally and thermomechanically must aim to be controlled in order to achieve predictable endpoints without creating collateral damage. As such, simultaneous confinement of heat and of the cavitation bubbles, in the vicinity of the targeted area, is desired.

Selective retina therapy (SRT) [1–6,8,12,15–18,22,24–26] represents a particularly relevant application where such damage confinement is critical. SRT has been introduced as an alternative to classical photocoagulation, a widely employed therapy for the treatment of different macular diseases [38]. Despite its efficacy, laser-directed photocoagulation can have adverse effects on the visual acuity of the patient due to the irreversible thermal destruction of photoreceptors. This is a result of the long exposure times (2-100 ms) that are typically employed in this procedure, that can produce significant heat conduction between the RPE and the neural retina [22,39]. The rationale of SRT is to confine damage to the RPE layer using shorter (~microsecond) exposure times, with the destroyed cells being presumably replaced by the subsequent migration and proliferation of neighboring healthy cells [3,5,23,40,41]. For laser pulse duration shorter than a few µs, microcavitation around melanosomes of the RPE cells becomes the dominant mechanism of cell injury [5,9–11,13,14,42]. From a clinical perspective, it is crucial that bubble size reproducibility and control are ensured during SRT treatments for confining damages to the RPE layer and for sparing adjacent healthy photoreceptors, which is required to preserve the visual function of the patients. It is therefore of prime importance to understand the impact of the irradiation conditions on heat diffusion and on thermomechanical cavitation bubble formation dynamics in the context of SRT in order to ensure truly selective targeting of the RPE.

Background work examining the influence of time-domain irradiation parameters on the spatial extent of thermal and thermomechanical damage produced by microcavitation has mainly focused on the impact of the laser pulse duration [5,8,12,15–17,19,21,43–47]. From these studies, it is now well established that as the pulse duration is reduced from the microsecond to the nanosecond range, the threshold radiant exposure to initiate microcavitation around melanosomes is also reduced because of improved thermal confinement. Indeed, as the pulse duration becomes shorter than the characteristic heat diffusion time within a melanosome (<1 µs), steeper temperature gradients can be produced and the critical temperature for bubble formation via explosive vaporization can be reached at the surface of the melanosomes with less energy delivered to the tissue, compared to longer pulses. For individual pulses in the sub-nanosecond regime, bubble generation can be triggered at even lower radiant exposures when stress confinement conditions are met (stress-confined bubble generation instead of explosive vaporization). In the case of melanosomes, stress transients originating from thermoelastic effects become relevant for pulse durations below 100 ps [48,49]. Nanosecond and picosecond pulses are therefore more attractive than microsecond pulses from a purely thermal point of view, because microcavitation can be triggered with lower levels of laser energy and with better spatial confinement of thermally-induced damage. However, the total volume of tissue altered by microcavitation is not solely determined by this photothermal contribution. Bubble expansion and collapse can create damage beyond the thermally affected region.

In microcavitation experiments carried out with suspensions of porcine melanosomes in water, Neumann and Brinkmann reported [4,16,17] that short (e.g. 12 ns) pulses produced a steep increase in the average bubble size with radiant exposure, while longer (e.g. 0.24 and 1.8 µs)

Biomedical Optics EXPRESS

pulses yielded a self-limited, constant bubble size over a certain range of radiant exposures above threshold. These results suggest that the benefit of using shorter pulses from a thermal perspective can be outweighed by more explosive vaporization that can limit control over the volume of tissue altered thermomechanically. When considering solely the thermomechanical damage, microsecond pulses are preferable since bubbles of a limited volume can be produced without a strong dependency over the applied radiant exposure. This represents a safer option for clinicians in the context of variability in eye transmissions and pigmentation levels from patient to patient. As such, SRT procedures currently rely on laser pulses having a duration of ~ 1.7 µs, mainly to limit the risk of scotoma (partial vision loss) and/or bleeding associated with the lack of control over the volume of the cavitation bubbles produced by short nanosecond pulses. Conversely, the use of microsecond pulses involves a sacrifice on the thermal confinement of damages. Since melanosomes tend to gather on the apical side of the RPE [5,50,51], close to the RPE-photoreceptor interface, the distance between individual melanosomes and the photoreceptors can be as small as 1 µm or even in the sub-µm range. With typical heat diffusion rates of roughly 1 µm/µs in tissues [22], the risk of photothermal damage to the fragile photoreceptors is expected to grow when employing pulses longer than 1 µs. Therefore, it seems reasonable to hypothesize that the optimal therapeutic bandwidth for SRT will be obtained with pulse duration of a few hundreds of nanoseconds, where the crossover from photothermal to thermomechanical damage is expected to take place. However, a relatively limited amount of data is available in this range [5,8,44,45], maybe due to the limited flexibility of Q-switch lasers having been employed so far. Thus, optimal pulse characteristics remain unknown.

The concept of pulse duration gives limited information about rates of laser energy deposition in tissues, such rates being actually determined by the pulse amplitude profile or shape. The recent advent of nanosecond and picosecond fiber lasers with flexible pulse formats [52–57] opens up new opportunities for improving control and precision in laser treatments involving microcavitation. Pulse shape tailoring can be used to finely adjust the rate of energy coupling in tissues and can, in principle, be tuned to generate ideal temperature fields allowing for a precise control of both heat diffusion and the kinetics of vaporization, thereby optimizing thermomechanical confinement.

The aim of this study is to investigate the effects of temporal shaping of nanosecond laser pulses and picosecond laser pulse trains on cavitation thresholds and bubble dynamics around melanin granules and retinal melanosomes. To the best of the authors' knowledge, no experimental results on the impact of the pulse shape on laser-directed microcavitation have been reported so far in the sub-microsecond regime.

2. Materials and methods

2.1. Melanin granules sample preparation

A few milligrams of melanin from Sepia officinalis (Sigma-Aldrich Co. LLC) were resuspended in distilled water and vortex-mixed for 20 s at 2500 rpm. Using a syringe, 2-3 drops of the suspension were deposited on a microscope slide. The sample was then sealed with a cover slip and vacuum grease. Examination of a typical sample by scanning electron microscopy (SEM) reveals the presence of granules having diameters ranging from <1 µm to a few tens of microns. It was also found that although roughly spherical in shape, the granules possess some depressions or crevices and are in fact compact aggregates of smaller sub-units or monomers having a typical diameter of ~150 nm.

2.2. Preparation of RPE melanosome suspensions

Freshly enucleated bovine and leporine (rabbit) eyes were obtained from local slaughterhouses. The eyes were cut equatorially and both the vitreous and the neural retina were removed from

Biomedical Optics EXPRESS

the posterior hemisphere to expose the RPE. To extract the melanosomes, the RPE was scraped mechanically while in a bath of distilled water (osmotic shock). Few drops of the melanosome suspension were deposited on a microscope slide and sealed with a coverslip and vacuum grease.

2.3. Pump-probe setup

A pump-probe setup (Fig. 1) was built around an inverted microscope (Nikon Eclipse TE2000-U). Isolated melanin granules and melanosomes were irradiated in single shot mode at 532 nm in two series of experiments using a frequency-doubled fiber laser platform (INO MOPAW) offering programmable pulse shapes. The energy per pulse being transmitted to the sample was controlled with a variable attenuator (rotating half-wave plate followed by a Glan-Taylor polarizer), its value was determined using a joulemeter (Coherent model J-10SI-LE). The pulse amplitude profile was monitored with a photodiode (EOT ET-4000).

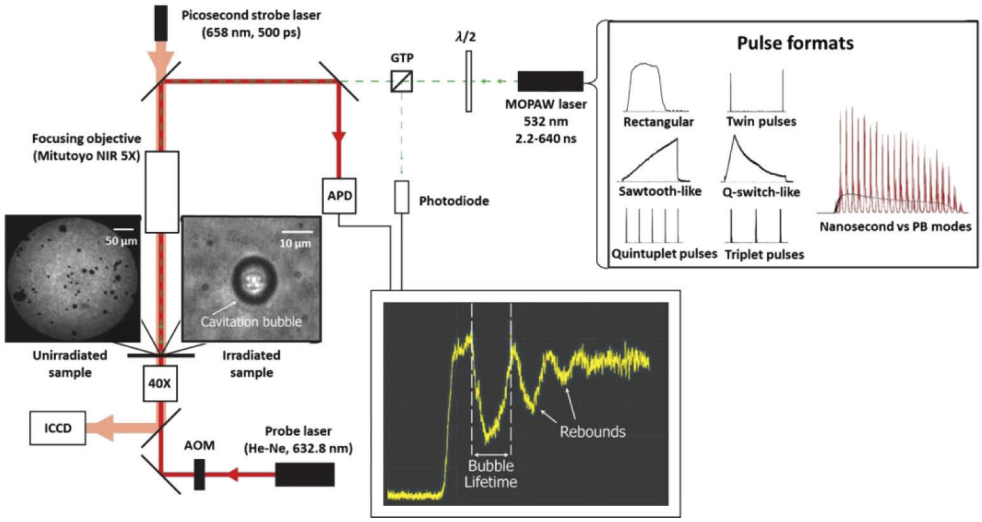

Fig. 1. Schematic representation of the pump-probe setup. AOM: acousto-optic modulator, APD: avalanche photodetector, ICCD: intensified CCD camera, GTP: Glan-Taylor polarizer, $\lambda/2$: half wave plate (532 nm). The different pulse formats employed for the microcavitation experiments are shown in the inset at the right of the MOPAW laser. For the twin pulses, triplet pulses and quintuplet pulses formats, the sub-pulses have a duration of 2.2 ns FWHM. Sub-pulses in the triplet and quintuplet formats are evenly spaced. Also shown in the inset: comparison of the amplitude profiles in the nanosecond (black curve) and PB (red curve) laser operating modes for a given energy and pulse format (reprinted with permission from ref. 57). The durations employed for each pulse format and laser operating mode can be found in Table 1.

The laser beam was focused onto the sample using a 5X objective (Mitutoyo 5X M-Plan NIR), which yielded an approximately Gaussian laser spot with a $1/e^2$ diameter of ~ 18 µm at focus. Cavitation bubbles around individual particles were observed by means of time-resolved imaging using a 40X microscope objective, a strobe illumination source (pulsed laser diode PicoQuant LDH series, former model LDH-8-1-1061, pulse duration ~ 500 ps, pulse energy ~ 125 pJ, full width at half maximum (FWHM) spectral bandwidth of 3 nm) and a gated ICCD camera (Andor iStar DH734-18U-A3). The strobe source was coupled in a multimode fiber (100 µm core diameter) whose output was imaged on the sample to produce a uniform illumination field having a diameter of ~ 330 µm. The delay between the laser trigger signal and the strobe source trigger signal was adjusted to visualize cavitation bubbles at different instants following the arrival of the laser pulse at the sample.

Biomedical Optics EXPRESS

Table 1. Pulse durations (given in nanoseconds) employed in the experiments involving differing pulse formats[a], laser operating modes and sample types.

		Laser operated in nanosecond mode		Laser operated in picosecond burst (PB) mode
Pulse format	Melanin granules	Bovine melanosomes	Leporine (rabbit) melanosomes	Leporine (rabbit) melanosomes
Rectangular	2.3-300		530	530
Twin pulses	5-630			
Sawtooth-like	300, 630	300, 630	530	530
Q-switch-like	2.2-630	2.2-630	530	530
Quintuplet pulses	630	630		
Triplet pulses	630			

[a]See also Fig. 1.

To measure the cavitation bubble lifetime, τ_{bubble}, the setup also included a counter-propagating He-Ne probe beam and an avalanche photodetector (APD, Thorlabs APD110A) to measure the probe transmission with a temporal resolution of 50 ns. Similar setups have been employed in earlier experiments to study cavitation bubble dynamics (see for instance reference 36). The probe beam was chopped synchronized to the laser pulses with an acousto-optic modulator (AOM, Newport Corp. model EOS N23080) to limit the probe irradiation time to a few microseconds in order to limit heating of the particles. Also, a variable beam expander allowed for adjusting the probe beam diameter at the sample to maximize the bubble detection sensitivity. The APD signal (probe transmission) and the photodiode signal (irradiation pulse shape) were recorded by a digital oscilloscope (Tektronix MDO 4104-3). All irradiations were carried out with a single melanin granule or a single melanosome present and centered within the 18 µm laser spot.

2.4. Irradiation conditions in the time domain

In a first series of experiments, six different pulse formats (Fig. 1) with duration ranging between 2 and 630 ns were employed to irradiate bovine melanosomes and melanin granules in single shot. Here the term format denotes a *type* of pulse temporal shape or intensity profile in the time domain (range of 2-630 ns), regardless of its duration. For instance, the laser can be programmed to produce sawtooth-like pulses of differing durations lying between 2 ns and 630 ns to investigate the relationship between the cavitation threshold and the pulse duration for the sawtooth-like format. In a second series of experiments, a "picosecond burst" (PB) mode was employed. In the PB mode, compact trains of picosecond pulses can be generated, the shape of trains being programmable over the same temporal range than in the "regular" nanosecond mode just described. In other words, the laser can be programmed to produce trains of picosecond pulses, the format (type of amplitude profile) of the trains being adjustable over a range of durations of 2-630 ns. The picosecond sub-pulses are evenly spaced in time (550 ps period) and have a typical full width at half maximum (FWHM) of 60 ps, which lies in the range of durations where thermoelastic effects become relevant for melanosomes [48,49]. Figure 1 compares nanosecond and PB modes for a given pulse format in terms of the emitted peak power for the same total energy. Typically, the peak power is $4-5$ times higher in the PB mode [57], compared to the nanosecond mode. By comparing experiments in both the nanosecond and the PB mode observations about the impact of the peak power and the effect of stress confinement on the cavitation threshold and on the bubble dynamics are extracted. Three pulse formats (rectangular, sawtooth-like and Q-switch-like) with the same duration (530 ns) were employed to irradiate

Biomedical Optics EXPRESS

leporine melanosomes in both modes of emission. In the PB mode, each train was formed of about 969 sub-pulses, the average radiant exposure produced by a sub-pulse at the cavitation threshold being of the order of 100-200 μJ/cm^2 at the focal point. Table 1 presents a summary of the durations employed for each pulse format, laser operating mode and sample type in both series of experiments.

2.5. Determination of radiant exposure

All values of the radiant exposure H for the irradiation (mJ/cm^2) correspond to the experimentally determined peak radiant exposure at the sample (at the center of the irradiation laser beam). The peak radiant exposure was calculated from the measured energy per pulse (see section 2.3) and the spatial intensity profile measured at the sample plane with the ICCD camera, after background subtraction.

2.6. Thermal modeling

The evolution of the temperature field within and around the particles upon irradiation was modeled using Matlab (version R2013a, MathWorks). The numerical model considered spherical particles of homogeneous composition within a homogeneous and transparent medium, and was built around an extension of Goldenberg and Tranter's solution [58] of the heat equation,

$$\frac{\partial T}{\partial t} - \kappa \nabla^2 T = \frac{A}{\rho c_p} \tag{1}$$

where T is the temperature increase, κ is the thermal diffusivity, ρ is the density, c_p is the specific heat and A is the energy uptake per unit volume and per unit time by the particle. Although Goldenberg's solution applies for a constant source term, it can also be employed to compute the solution for a time-dependent source term [15], as occurring in particle heating driven by laser pulses having arbitrary temporal shapes. The method relies on finding the impulse response of the system and doing a convolution of that impulse response with the time dependent source term. This solution assumes homogeneous spatial heating of the particles. Therefore, only a radial dependency of the calculated temperature distribution is provided at any given time. Since non-uniform, approximately gaussian beam profiles were employed to irradiate the particles, heating was not perfectly homogeneous in a plane normal to the beam axis. This was accounted for in the calculation of the energy uptake by the particles by performing integration of the fluence over the beam radius, assuming a Gaussian beam profile and employing an approach similar to that of Gerstman et al. [9].

3. Results

3.1. Cavitation threshold – experimental results

At the cavitation threshold radiant exposure, H_T, a small dip appears in the probe transmission signal, toward the end of the laser pulse. Time-resolved images taken in this condition typically reveal nucleation of a bubble starting at a given site on the surface of the melanin granules (Fig. 2(A)), as also reported for other types of particles in previous work [15,59].

As shown in Fig. 2(B), the threshold was found to be independent of the size of the melanin granules (range 1-5 μm in diameter), which further suggests that local, submicronic surface phenomena dominate the onset of microcavitation, as opposed to global processes involving the whole granules. For melanosomes, the spatial resolution of the setup was not sufficient to visualize localized nucleation sites.

Figure 3(A) summarizes the results obtained for the cavitation threshold radiant exposure in the nanosecond mode. For each data point, the threshold was determined from a probit fit on data sets including measurements carried out with a least 20 particles. An example of such a fit is shown in

Biomedical Optics EXPRESS

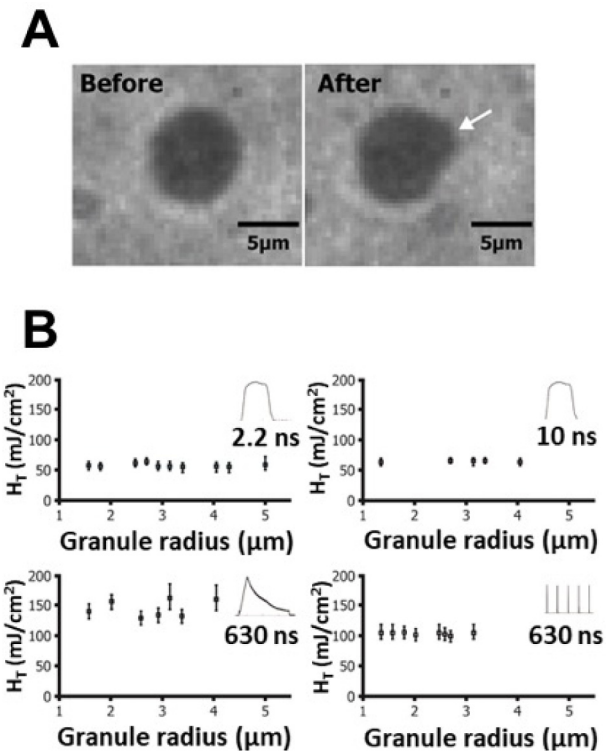

Fig. 2. Cavitation threshold results in the nanosecond mode with melanin granules. A) Time-resolved images showing a melanin granule before and 100 ns after irradiation by a single laser pulse (pulse format: rectangular, pulse duration: 300 ns), showing a localized nucleation site (arrow). B) Measured cavitation threshold radiant exposure (H_T) for individual granules as a function of the granule radius for different pulse formats.

Fig. 3(B). As can be seen in Fig. 3(A), the impact of the pulse format grows with increasing pulse duration, especially above 50 ns. Differences of up to ~ 40% exist for a pulse duration of 630 ns. For both the melanosomes and the melanin granules, the Q-switch-like pulse format yielded the highest threshold radiant exposures (and thus the poorest thermal confinement). The comparative cavitation threshold radiant exposure measurements performed in the nanosecond and PB modes for leporine melanosomes (not shown) revealed no significant differences between both modes, for all three tested pulse formats. The sawtooth-like format yielded the lowest threshold values in both modes of operation of the laser.

3.2. Threshold modeling results – surface temperature vs melanin particle radius

Figure 4 shows the numerically determined temperature elevations at the surface of spherical melanin particles in water as a function of their radius, when irradiated by pulses of differing formats at the experimentally determined threshold radiant exposures for melanin granules (Figs. 4(A) and 4(B)) and bovine melanosomes (Fig. 4(C)). The values listed in Ref. [15] were assumed for the thermal properties of water and melanin. In general, the temperature was found to be dependent on the radius of the particles.

In Fig. 4(A), the coefficient of absorption μ was set to 2370 cm^{-1}, corresponding to the value published by Jacques et al. [60], which yielded an average maximum temperature elevation of only (18 ± 4) K. This is obviously far from being sufficient to initiate vaporization, which requires *at least* ΔT ~100 K [61] and more likely ΔT ~120-130 K [5,11,15,59]. The model

Biomedical Optics EXPRESS

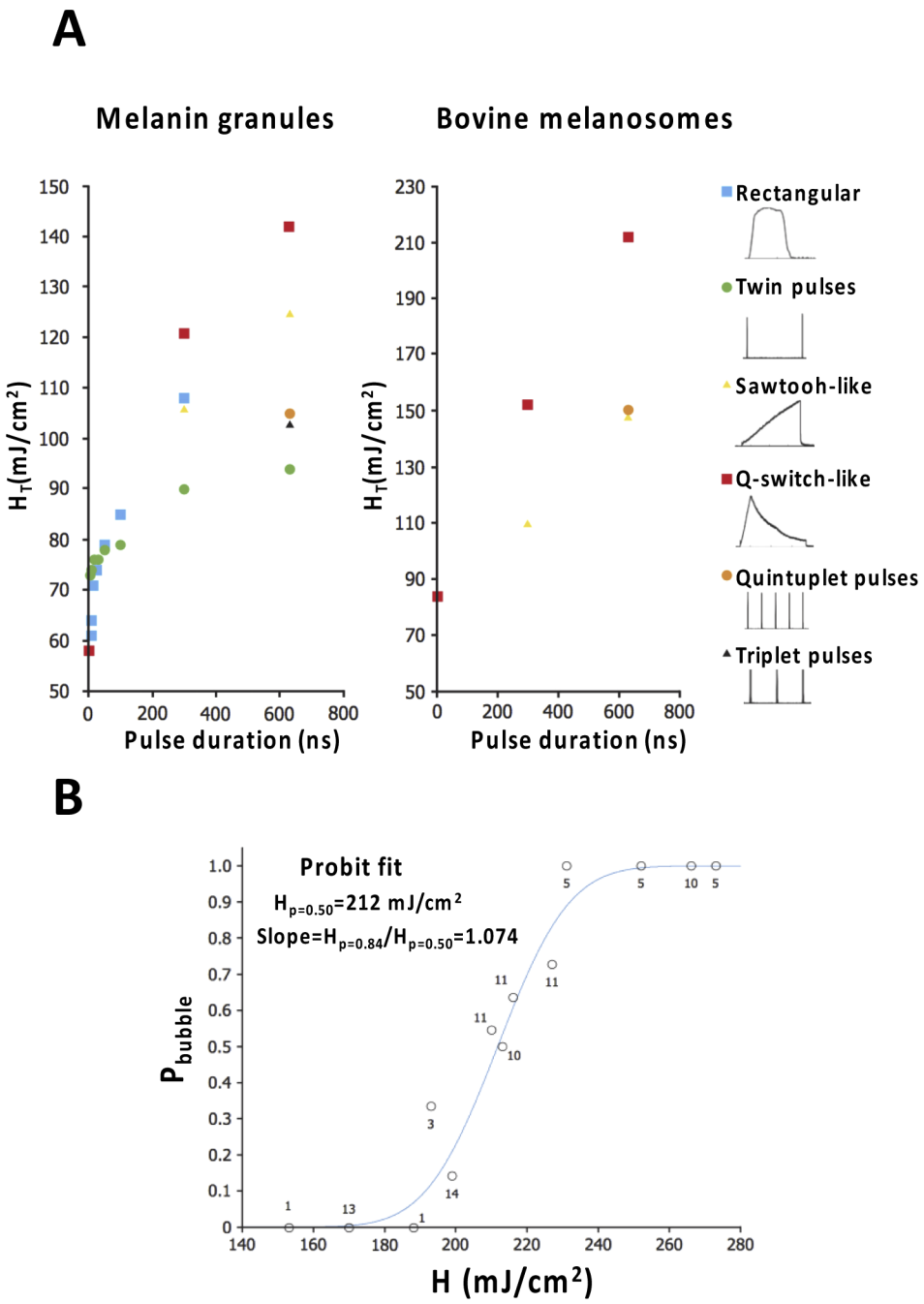

Fig. 3. Cavitation threshold results in the nanosecond mode – influence of the pulse format. A) Cavitation threshold radiant exposures measured as a function of pulse duration with differing pulse formats, for melanin granules and bovine melanosomes. B) Bubble onset probability P_{bubble} measured as a function of radiant exposure for bovine melanosomes with the Q-switch-like pulse format (duration: 630 ns). The numbers at the data points indicate the number of measurements performed to determine P_{bubble} at a given radiant exposure. Total number of measurements: 100 (n = 100), on 92 different melanosomes (N = 92). The probit fit yielded H_T = 212 mJ/cm^2 in that specific example.

Biomedical Optics EXPRESS

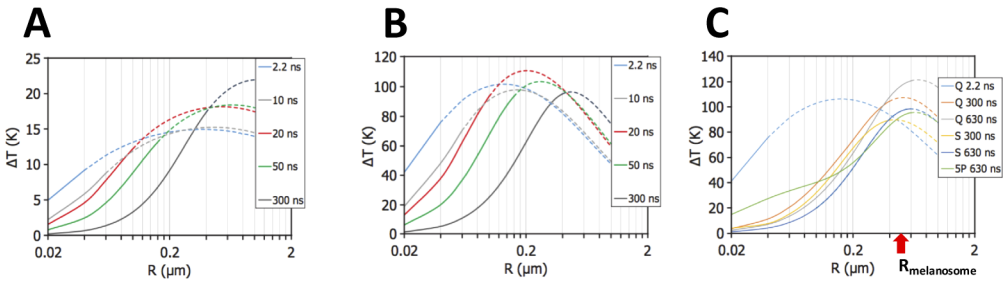

Fig. 4. Calculated surface temperature elevation of spherical melanin particles in water vs particle radius R upon irradiation with rectangular pulses of differing duration (color legend), at a radiant exposure corresponding to the experimentally determined cavitation threshold for melanin granules, assuming $\mu = 2370\,\mathrm{cm}^{-1}$ (A), and $\mu = 20\,000\,\mathrm{cm}^{-1}$ (B). For the dashed portions of the curves, the thermal confinement condition $\tau_p < R^2/4\kappa$ is fulfilled. C) Same calculation, for different pulse formats, at a radiant exposure corresponding to the experimentally determined H_T for bovine melanosomes and with μ set to a value ($13500\,\mathrm{cm}^{-1}$) yielding an average maximum temperature elevation of 100 K. Q denotes the Q-switch-like pulse format, S the sawtooth format and 5P the quintuplet pulse.

predicts that a minimum value of $\mu \approx 20\,000\ \mathrm{cm}^{-1}$ is required to produce a temperature rise of 100 K (Fig. 4(B)).

For melanosomes, a minimum value of $\mu = 13500\ \mathrm{cm}^{-1}$ is predicted to reach ΔT ~100 K in average. However, as shown in Fig. 4(C), the radius at which the maximum temperature increase occurs is found to depend on the pulse shape and duration and does not generally correspond to $R_{melanosome}$ (≈ 0.5 μm, indicated by the red arrow).

3.3. Microbubble dynamics

3.3.1. Single vs train of short nanosecond pulses

Figure 5 compares the bubble volume evolution with radiant exposure for a single short nanosecond pulse and a train of five such short pulses (quintuplet pulse format, see Fig. 1). The maximum volume V_{max} of the bubble (at the end of its expansion) is calculated from its radius r_{max}, which is first estimated (neglecting the role of surface tension) from the measured bubble lifetime τ_{bubble} using Rayleigh's equation,

$$r_{max} \approx \frac{\tau_{bubble}}{1.83}\sqrt{\frac{p_\infty - p_{sat}(T_\infty)}{\rho(T_\infty)}} \tag{2}$$

where p_∞ is the ambient pressure (101 kPa), $p_{sat}\ (T_\infty)$ the saturated vapor pressure at ambient temperature (2.33 kPa at $T_\infty = 293$K) and $\rho(T_\infty)$ the density of water (1000 kg/m^3). Then, the correction factor given in Ref. [36] is applied to account for surface tension effects and avoid significant underestimations of the bubble size for $\tau_{bubble} < 1$μs. As evidenced in Fig. 5, the bubble volume was found to increase very steeply with radiant exposure, as also reported by Neumann and Brinkmann [16,17], whereas much smaller bubbles are produced above threshold with the quintuplet. For the single pulse, the probe transmission data reveals a single bubble whose lifetime increases with radiant exposure, as opposed to the pulse trains, where several bubbles having shorter lifetimes can be produced, as shown in Fig. 6.

3.3.2. Q-switch-like vs sawtooth-like pulse formats (nanosecond regime)

Figure 7 demonstrates that for a given pulse duration, the pulse format can significantly affect the microcavitation dynamics and the resultant bubble size above the threshold. For bovine melanosomes and pulse widths τ_p of 300 ns (Fig. 7(A)) and 630 ns (Fig. 7(B)), the average bubble

Biomedical Optics EXPRESS

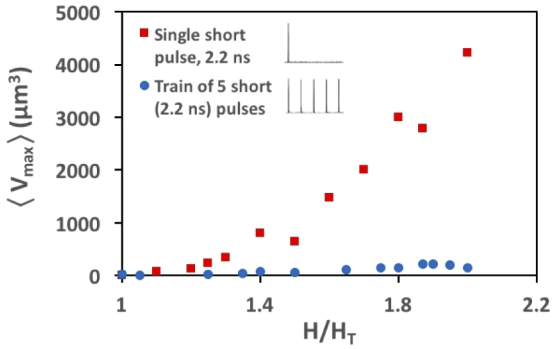

Fig. 5. Average maximum bubble volume ⟨Vmax⟩ as a function of the relative radiant exposure above threshold for a single and a train of 5 short (2.2 ns) pulses (bovine melanosomes). The pulse train duration is 630 ns (157.5 ns delay between consecutive pulses). For each data point, the average volume was calculated from at least 5 measurements (n = 5).

volume grows substantially faster with radiant exposure for the Q-switch-like shape, compared to the sawtooth-like shape, especially for $H > 1.4H_T$. For $\tau_p = 630$ ns, the sawtooth-like format produced bubbles whose volume is nearly independent of radiant exposure in the range of $1H_T$ to $2H_T$. For that same pulse duration at $H = 2H_T$, an order of magnitude difference was noticed in the average volume of the bubbles generated with these pulse formats.

Interestingly, two different signatures were found in the probe transmission data (total number of irradiated melanosomes = 109) for the Q-switch-like format and $\tau_p = 630$ ns (Fig. 7C). For 80% of the cases, the τ_{bubble} increases with radiant exposure, with some rebounds noticed mainly for $H > 1.5H_T$. For the remaining 20%, the self-limited bubble growth behavior reported by Neumann and Brinkmann [16] was observed.

3.3.3. Microbubble dynamics: nanosecond vs picosecond burst modes

Microcavitation experiments were conducted with leporine melanosomes, using the Q-switch-like and the sawtooth-like pulse formats in both the nanosecond and the PB modes, for radiant exposures up to $1.8H_T$. For these experiments the pulse (or burst) width was fixed (τ_p=533 ns), and a least 25 different melanosomes were individually irradiated for each condition. No significant differences in the bubble volume were found between the PB and the nanosecond regimes, the volume being essentially determined by the format employed (shape of the temporal envelope of the pulse or burst, either Q-switch-like or sawtooth-like envelope). These results suggest that thermoelastic stress has little or no influence on the microbubble dynamics when using picosecond pulse trains and the irradiation conditions that were employed during the experiments. As will be discussed in section 4, this result can be interpreted by considering the differences in the influence of stress confinement on phase transitions between single energetic pulses and bursts of low-energy pulses.

Biomedical Optics EXPRESS

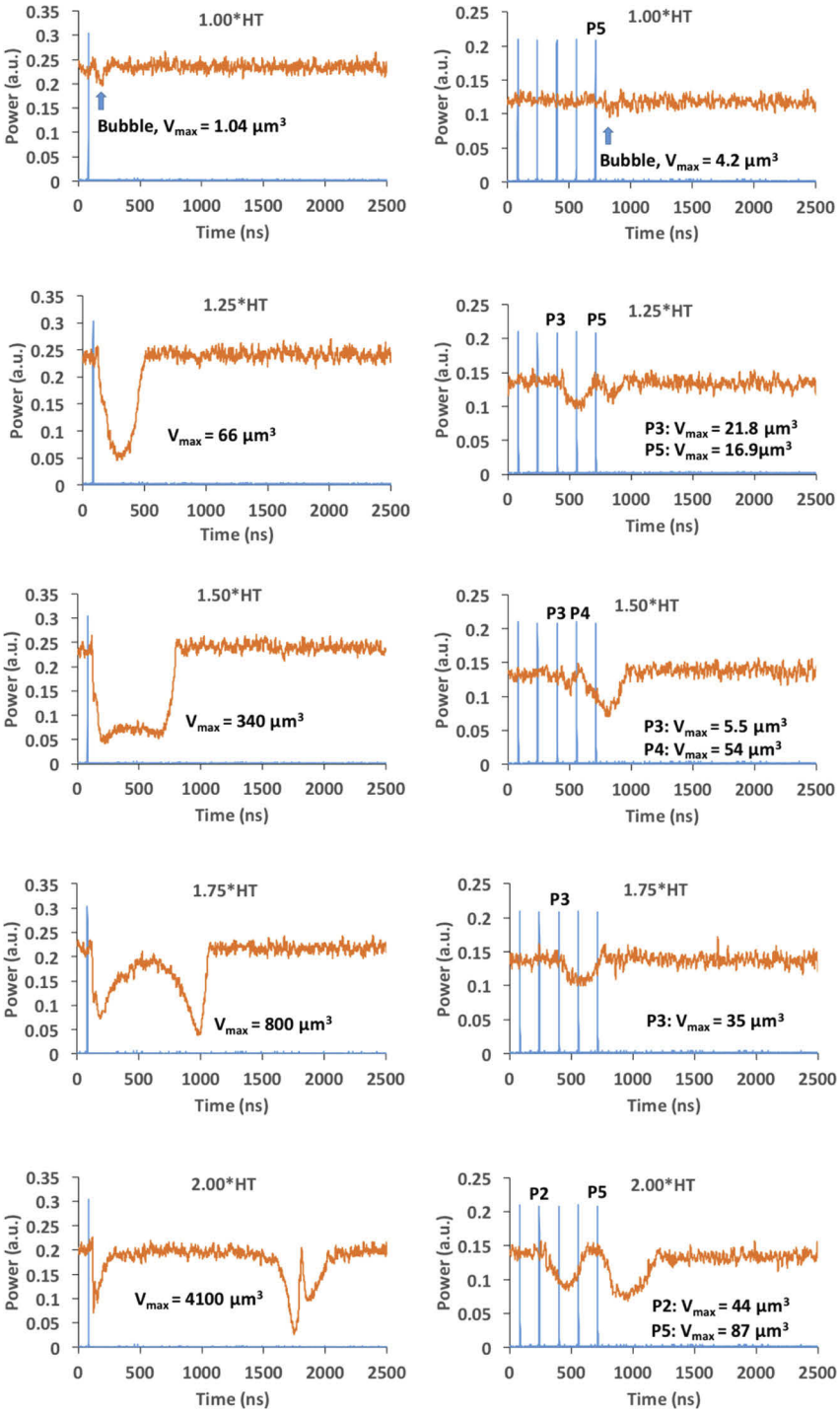

Fig. 6. Typical bubble dynamics around bovine melanosomes for a single (left column) and a train of (right column) 5 short pulses (2.2 ns each). Blue curves: laser pulse, orange curves: transmitted probe. For each bubble, the maximum volume V_{max} is indicated. Right column: P2, P3, etc. denotes bubble incipience at pulse 2, 3, etc.

Biomedical Optics EXPRESS

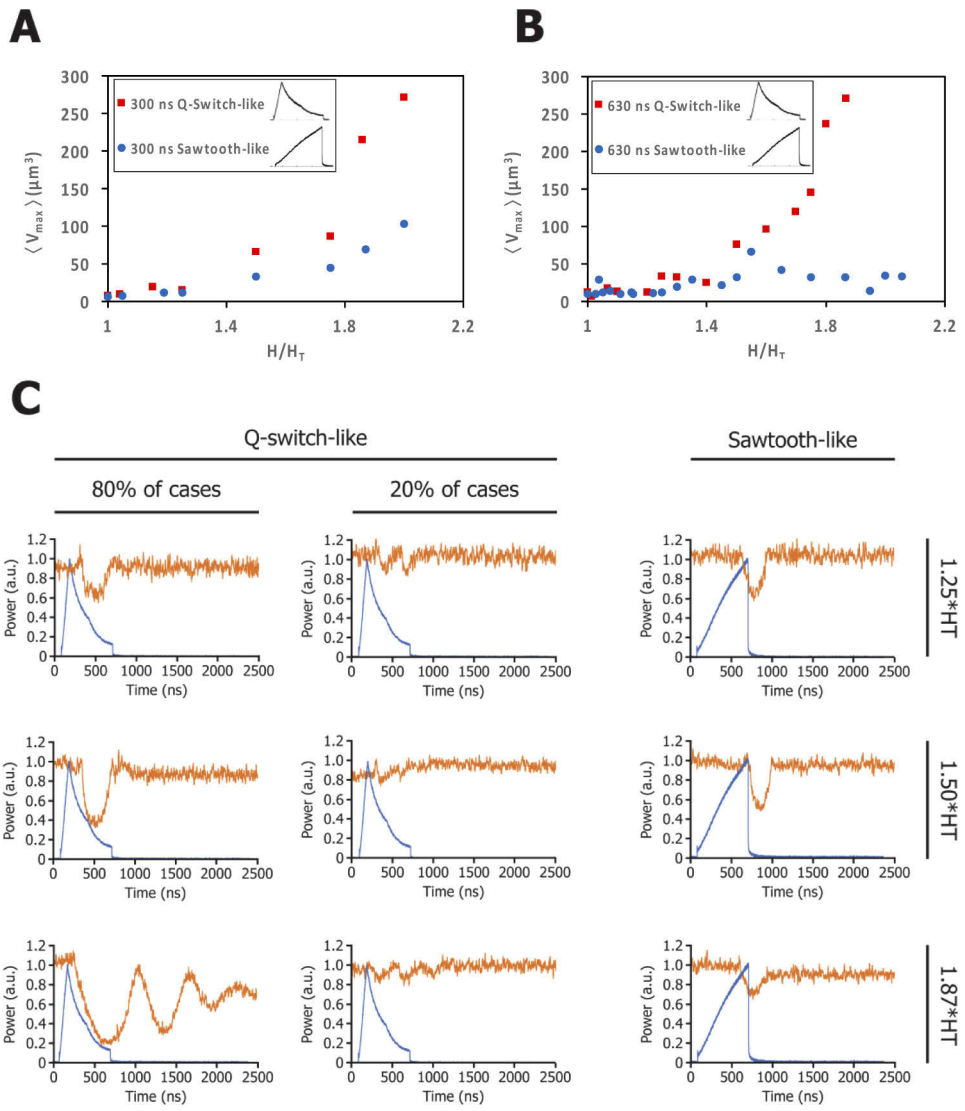

Fig. 7. A) and B) Average maximum bubble volume ⟨Vmax⟩ as a function of the relative radiant exposure above threshold for two different pulse formats (Q-switch–like, sawtooth-like), measured with bovine melanosomes. A) $\tau_p = 300$ ns, B) $\tau_p = 630$ ns. For each data point, the average volume was calculated from at least 5 measurements. C) Typical bubble dynamics around bovine melanosomes at different radiant exposures for Q-switch-like vs sawtooth-like pulse formats and $\tau_p = 630$ ns. Blue curves: laser pulse, orange curves: transmitted probe. Top row: $H = 1.25*H_T$, middle row: $H = 1.50*H_T$, bottom row: $H = 1.87*H_T$. Two different dynamics were observed with the Q-switch-like format, including the self-limited bubble growth reported by Neumann and Brinkmann [16], which represented 20% of the cases (22 out of 109 irradiated melanosomes).

Biomedical Optics EXPRESS

4. Discussion

4.1. Cavitation threshold – nanosecond regime

The impact of the pulse shape on the cavitation threshold as a function of pulse duration can be interpreted using semi-quantitative reasoning. The particle's surface temperature is dependent on the balance between the heating and cooling rates. Depending on this balance, more or less laser energy is required to reach the nucleation temperature. For heating rates much shorter than the cooling time, the pulse shape has negligible effect on the threshold because heating dominates and negligible thermal losses occur during the pulse, regardless of the shape. Contributions from pulse shaping increase when the particle heating rates become comparable to the particle's characteristic thermal relaxation time τ_{th} given by

$$\tau_{th} = \frac{R^2}{4\kappa} \tag{3}$$

where R is the particle radius and κ the thermal diffusivity. As evidenced in Fig. 3(A), the influence of the pulse shape on the threshold becomes significant for $\tau_p > 50$ ns. If this transition is assumed to match the condition $\tau_p \approx \tau_{th}$, then from Eq. (3) a particle radius lying between 160 and 240 nm is found, using the values (with κ lying between 1.22×10^{-7} m^2/s and 2.96×10^{7} m^2/s) that were reported [15,62,63] for the thermal diffusivity of melanin. This is smaller than the radius of the melanin granules irradiated in this study and also smaller than a typical melanosome ($R_{melanosome} \approx$0.5 µm). This seems consistent with the observation of localized nucleation sites at the surface of the particles and threshold values independent of the radius of melanin granules when in the range 1-5 µm (Fig. 2).

Qualitative arguments can also be employed for the interpretation of the pulse shape related differences in threshold radiant exposures for a given pulse duration. For example, consider the Q-switch-like vs the sawtooth-like shapes. With the Q-switch-like shape, most of the heating occurs at the beginning of the pulse, leading to early establishment of a significant temperature gradient between the particle and its surroundings. Conversely, with the sawtooth-like shape, most of the temperature gradient is created towards the end of the pulse (that is, right before bubble incipience when at threshold). Since the heat flow escaping from the particle grows proportional to this gradient, the energy delivered to the surroundings during the pulse is more important with Q-switch-like profiles than for sawtooth-like profiles. Therefore, reaching the nucleation temperature requires more energy with the former, hence a higher threshold radiant exposure.

4.2. Cavitation threshold – picosecond burst regime

Deconstructing nanosecond pulses ($\tau_p = 533$ ns) in trains of picosecond sub-pulses was found to have no measurable impact on the cavitation threshold. The stress confinement time τ_s is given by

$$\tau_s = \frac{2R}{c_s} \tag{4}$$

where R is the particle radius and c_s the speed of sound in the particle.

For a melanosome with $R = 0.5$ µm, $\tau_s \approx 700$ ps, assuming c_s=1500 m/s for melanin [15]. Since the duration of each individual sub-pulse is 60 ps in the PB mode, the thermoelastic expansion of the melanosome cannot dissipate energy fast enough to prevent a pressure buildup during a sub-pulse. Depending on their amplitude and duration, pressure transients can potentially affect the cavitation threshold, since the nucleation temperature is pressure-dependent, as pointed out by Neumann and Brinkmann [59]. In particular, the tensile part of the transients can induce bubble formation even for temperatures much lower than required for explosive vaporization [35–37,49]. A crude estimate of the amplitude and duration of the pressure transients can be calculated using

Biomedical Optics EXPRESS

the homogeneous and linearized model proposed by Sun and Gerstman [64]. Using this model, it can be shown that a single sub-pulse in the PB mode would produce a pressure an order of magnitude larger than that generated by the entire pulse envelope in the nanosecond mode. For the typical radius of a melanosome (R = 0.5 μm), the calculated stress in the PB mode is in the range of 350 – 439 kPa. These pressures are comparable to the saturated vapor pressure for nucleation temperatures lying between 411K and 419K, which are typical for melanosomes [11,15,59]. Now, the amplitude of tensile wave depends on the acoustic impedance mismatch at the melanin-water interface. Using the reasoning and assumptions of Jacques et al. [65] the tensile stress produced by an individual sub-pulse would be of the order of only 21-26 kPa, which is quite low compared to the threshold stress of 800 kPa for cavitation bubble generation in aqueous solutions [65], and at least a factor of five smaller than the Blake threshold for heterogeneous nucleation with an initial bubble having the size of a melanosome [37]. Even a constructive superposition of two such tensile transients arising from two consecutive individual sub-pulses (separated by a time interval of 550 ps) would likely yield tensile stresses below the threshold. The fact that similar cavitation threshold values were found in the nanosecond and PB modes is indicative that the dynamics of bubble generation using bursts of low-energetic picosecond pulses (each meeting the stress confinement condition) will generally differ from the bubble generation mechanisms involved when using individual energetic picosecond pulses. As in the nanosecond mode, explosive vaporization likely dominated the bubble generation process in our experiments using the PB mode; most probably because each individual sub-pulses generated insufficient tensile stress to initiate a phase change (cold bubble generation). Nonetheless, the possibility of generating sufficient tensile stress in the PB mode to initiate cavitation with less energy delivered to the melanosome (compared to explosive vaporization-based bubble generation in the nanosecond mode) should not be ruled out. For instance, a series of n picosecond sub-pulses of equal energy could be delivered, the last one having just the energy required to produce the necessary tensile stress, considering the increase of the temperature-dependent Grüneisen coefficient Γ [37,65] arising from the heating of the melanosome by the first n-1 pulses. For the sake of example, consider ten consecutive 60 ps-sub-pulses of equal energy with a constant inter-pulse period of 550 ps (therefore a burst of ~ 5 ns), with a deposited energy of 32 J/cm^3 per sub-pulse, which is assumed sufficient to produce the tensile stress required to initiate bubble formation with Γ ~ 0.4 [65]. Each sub-pulse would generate a temperature jump of 8.5 K [65]. As the temperature increases by 8.5 K steps, Γ also increases by steps (starting from a value of ~ 0.1 at room temperature) until it reaches the value of 0.4 at the tenth sub-pulse, that is sufficient to initiate cavitation. In that example, the total temperature increase for the whole burst is 85K at most, which is not sufficient to trigger explosive vaporization, but the tensile stress produced by the tenth sub-pulse is sufficient for thermoelastically-driven bubble generation. At threshold, the total deposited energy (burst energy) is 320 J/cm^3, which, for the coefficient of absorption of 12 000 cm^{-1} experimentally determined in this work for melanosomes, corresponds to a radiant exposure of ~ 27 mJ/cm^2, a value lower than the explosive vaporizations thresholds (55- 120 mJ/cm^2)typically reported [5,11,15–17] for short nanosecond pulses at around 532 nm, including in this study. To produce the energy uptake mentioned in the above example, the radiant exposure of each sub-pulse needs to be about 20 times larger than it was during the experiments carried out in the PB mode. Since the above calculations are rough estimates, more sophisticated models and additional experimental work are needed to confirm or to invalidate these predictions. The experimental results obtained in the PB mode can also be discussed from the perspective that the PB mode allows for employing higher pulse peak power levels without noticeable impact on the bubble generation dynamics and bubble size dependency with respect to radiant exposure. This could turn out to represent an opportunity for improving the signal to noise ratio of photoacoustic dosimetry techniques for sub-microsecond laser eye surgeries, since in the PB mode a tenfold increase of the acoustic pressure levels is predicted, compared to the nanosecond mode, for the

Biomedical Optics EXPRESS

same delivered energy. Another advantage of working with higher peak power for a given energy is to improve the harmonic wavelength conversion efficiency when producing pulse trains in the visible region of the spectrum from lasers relying on an oscillator emitting in the near-infrared (where melanin absorption can be an order of magnitude lower compared to visible wavelengths [60,61]).

4.3. Modeling results – surface temperature vs melanin particle radius

For the curves of Fig. 4, the presence of a maximum ΔT_{max} is noticed for some radius R_{Tmax} that grows with pulse duration. The fact that R_{Tmax} is in general smaller than the typical radius of the granules that were irradiated in the experiments suggests that models considering local heating at the surface of the granules may be more relevant than models assuming homogeneous heating of the whole granule. Other authors discussed the possibility of hot spot structures in laser-heated melanosomes with local temperature rises an order of magnitude higher than the average melanosome temperature and local absorption coefficient as high as 36 000 cm^{-1} for an average melanosome absorption coefficient of 2 000 cm^{-1}[66]. Evidence of localized nucleation sites (Fig. 2(A)) and the observation of threshold radiant exposures being independent of the granule radius (Fig. 2(B)) further suggest that such local heating effects shall be considered to accurately model the temperature evolution and the onset of microcavitation at the surface of the particles.

4.4. Local heating model

To model the cavitation thresholds in the context of local heating using our adaptation of Goldenberg's solution, we considered spherical volumes of variable radii corresponding to a portion of the whole particle that is in contact with water, as shown in Fig. 8. For temperature calculations, the spherical volume was treated as an isolated particle in water, thus neglecting the influence of the rest of the melanin granule. This approximation appears reasonable if thermal confinement applies within the spherical volume and if the thermal conductivity $\kappa\rho c_p$ of melanin is close to that of water.

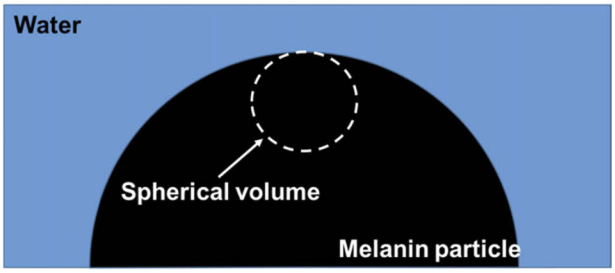

Fig. 8. Illustration of the local heating model for melanin particles. Only a spherical portion of the granule is considered in the calculations.

For a given pulse format, the rate of temperature increase dT/dH, where H is the radiant exposure, is calculated as a function of the radius of the spherical volume. A curve similar to the ones shown in Fig. 4 is then generated, with a maximum rate $(dT/dH)_{max}$ at a specific radius R_{Tmax}. The model then assumes that the cavitation threshold H_T is given by

$$H_T = \frac{T_{nuc} - T_{amb}}{(dT/dH)_{max}} \tag{5}$$

where T_{nuc} is the nucleation temperature, which is assumed constant for all pulse formats [15], and T_{amb} the ambient temperature. To fit the experimental thresholds for bubble formation, the model

Biomedical Optics EXPRESS

considers T_{nuc} and μ as free parameters. Since a single nucleation temperature is assumed for all irradiation conditions, the product of the experimental threshold with $(dT/dH)_{max}$ is expected to remain constant for all pulse shapes and duration. As such, a statistical criterion can be defined to determine the best fit values of T_{nuc} and μ for a given set of experimental thresholds, namely the minimum of the coefficient of variation ($C.V.$) of the quantity $H_T \times (dT/dH)_{max}$, given by

$$C.V. = std(H_T \times (dT/dH)_{max}) \div \overline{H_T \times (dT/dH)_{max}} \quad (6)$$

Figure 9(A) shows the corresponding modeled curves for rectangular pulses (with n = 35 threshold measurements with *Sepia* melanin granules), assuming thermal properties previously reported [15], where thermal conductivities of melanin and water differ by only 17%. The minimum $C.V.$ of 0.046 is found for $\mu = 18\,000$ cm^{-1} and $\overline{H_T \times (dT/dH)_{\max}} = 95$ K. Assuming $T_{amb} = 293$ K, Eq. (5) yields a nucleation temperature of (388 ± 4) K, which is close to the value of (385 ± 7) K published by Jacques and McAuliffe [61] for skin melanosomes, and reasonably consistent with the results reported by Neumann and Brinkmann ((409 ± 23) K) for retinal porcine melanosomes [15]. With these parameters entered in the model, the calculated thresholds for *Sepia* melanin granules are found to be in reasonable agreement (average error of 6.6%) with the experimental results, as shown in Fig. 9(B). The geometric simplicity of the model compared to the complexity and polydispersity of the structure of the granules might be at the origin of the discrepancies between the model and the experiment. More sophisticated models accounting for the actual topology and variances of the granules would be more reliable. Also, thermal confinement inside the spherical volume was assumed, which is only weakly fulfilled for some pulse shapes (Fig. 4(B)).

To fit the thresholds measured with bovine melanosomes, an upper limit of 0.5 µm was imposed for the radius of the spherical volume of Fig. 8, corresponding to the typical radius of a melanosome. Using again properties of Ref. [15] for melanin, a minimum $C.V.$ of 0.10 is found at $\mu = 12\,000$ cm^{-1}, with a nucleation temperature of $(387 \pm 9$ K), as illustrated in Fig. 10(A). Again, the resulting model's predictions for the threshold dependency on the pulse format closely match those of experimental results (Fig. 10(B)).

4.5. Bubble size vs radiant exposure

4.5.1. Pulse formats with multiple short sub-pulses vs single short pulse

The lowest thresholds were obtained with single short pulses of a few nanoseconds. Our results also confirm the quick increase of bubble size above threshold previously reported [4,16,17]. Our results further demonstrate that trains of such short pulses can be used to limit the growth in bubble size (Figs. 5 and 6), at the expense of a higher threshold (150 mJ/cm^2 vs 84 mJ/cm^2 for the cases shown in Fig. 6). Moreover, 150 mJ/cm^2 is about three times lower than reported thresholds for melanosomes irradiated with 1.8 µs long Q-switch pulse envelope that are typically employed in SRT procedures [4], and 1.8 times lower than 240 ns long Q-switch pulses [16].

To explain the bubble size limitation, first, the case of a pair of identical sub-pulses (twin pulses in Fig. 1) is considered. At cavitation threshold, a bubble is initiated at the second sub-pulse. Upon increase of the radiant exposure, the maximum size of this bubble increases (cavitation starting on the second sub-pulse). At a certain radiant exposure, the energy contained in the first sub-pulse becomes sufficient to initiate cavitation. Above that point, cavitation starts on the first sub-pulse, and the lifetime of any bubble initiated at the second sub-pulse could be limited to a maximal value. A possible explanation for this bubble dynamics is that a shielding effect of the bubble created at the first sub-pulse could be involved. As such, because bubbles can scatter and/or diffract light, they can shield absorption of laser light. For twin pulses, this would happen for radiant exposures such that the lifetime of the bubble initiated at the first sub-pulse is of the same order or larger than the delay between the two sub-pulses. The consequence

Biomedical Optics EXPRESS

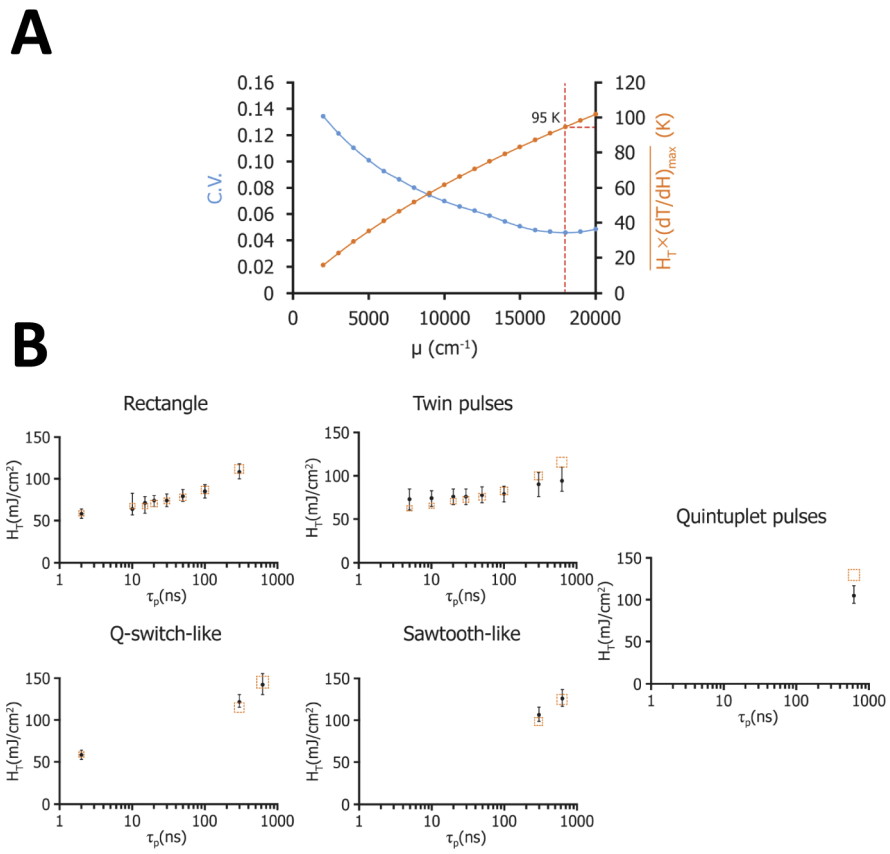

Fig. 9. Local heating model results for melanin granules. A) Model's predictions for the coefficient of absorption (18 000 cm^{-1}) and maximum surface temperature increase (95 K) at threshold for melanin granules irradiated by rectangular pulses having durations ranging from 2.2 ns to 300 ns. B) Calculated (squares) vs experimental (dots) threshold radiant exposures for melanin granules ($\mu = 18\,000\ cm^{-1}$, $T_{nuc} = 388 \pm 4$ K) irradiated with differing pulse formats. The height of the squares represents the uncertainty on the predicted values due to the uncertainty on the nucleation temperature.

is that the lifetime (and hence the volume, since they are related) of the bubble created at the second sub-pulse can be controlled so that it will not exceed a maximum value determined by the individual sub-pulse characteristics and by the time delay between them. This translates into a reset in dynamics of the maximum bubble size when increasing the radiant exposure, as shown in Fig. 11, for melanin granules. This reset extends the range of radiant exposures for which the bubble volume can be maintained smaller than a certain value, compared to irradiation with a single short pulse. This high level rationale can be generalized to pulse formats having more than 2 sub-pulses for interpreting the result of Fig. 6. In general, upon increase of the radiant exposure, multiple bubbles will be generated, with sizes and incipience times being determined by the interplay between the energy of the sub-pulse, their period and the magnitude of the shielding effects described above. Using ray optics, we have roughly estimated the loss of deposited energy in the absorber due to bubble shielding at 25% when considering a perfectly spherical bubble centered on a spherical absorber. In reality, the bubble can emerge from a localized site of non-spherical absorbers (see Fig. 2(A)) and scattering effects certainly come into play. More sophisticated models are therefore required to evaluate the amount of shielding with better

Biomedical Optics EXPRESS

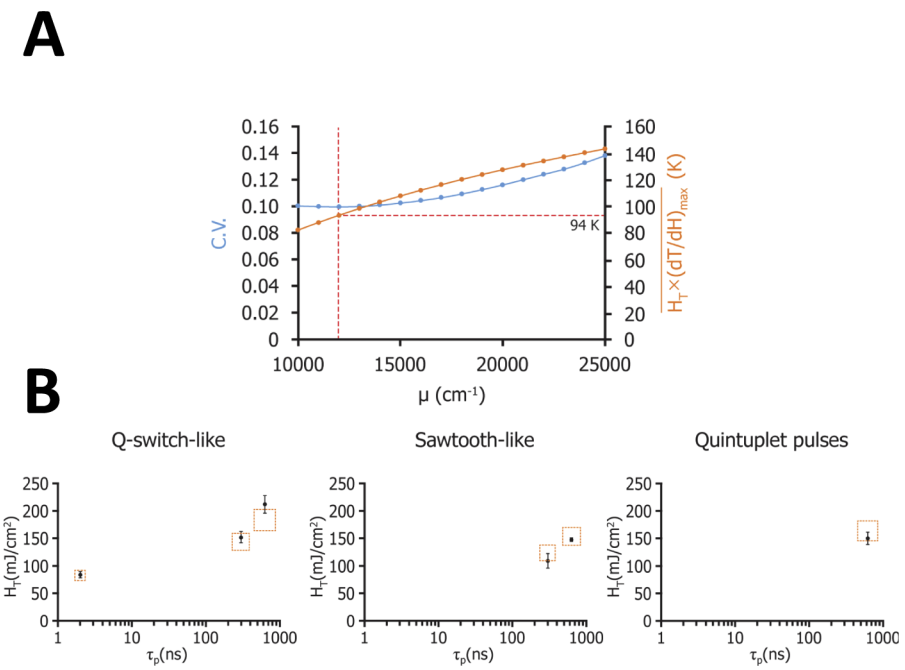

Fig. 10. Local heating model results for bovine melanosomes. A) The model's predictions for μ and the maximum surface temperature increase at threshold are 12 000 cm^{-1} and 94 K respectively. B) Calculated (squares) vs experimental (dots) threshold radiant exposures for bovine melanosomes ($\mu = 12\,000$ cm^{-1}, $T_{nuc} = 387 \pm 9$ K) irradiated with differing pulse formats.

accuracy. Another possible explanation for the absence of bubble formation after the second pulse at $H > 1.6\ H_T$ would be that the heating produced at the nucleation site is very localized (considering the short pulse duration of 2.2 ns, thermally-confined hot spots with diameters of less than 40 nm would be produced) and the temperature of the hot spot after the second pulse would have enough time to decrease below the nucleation temperature before the end of the collapse of the bubble generated after the first pulse, as a result of heat conduction within the whole melanin granule.

4.5.2. Sawtooth-like vs Q-switch-like pulse formats

As discussed in section 4.1, the higher threshold of the Q-switch-like pulse format is presumably a consequence of larger amounts of heat delivered to the water due to larger temperature gradients generated during the pulse, compared to the sawtooth-like format. Above threshold, the same phenomenon may also partly explain the observed shape-related differences in the bubble growth, since it can influence the volume of superheated, metastable water surrounding the particle. The latter determines the amount of energy stored in the medium that can be converted into bubble kinetic energy during bubble expansion. As the radiant exposure grows above threshold, the steeper temperature gradients generated with Q-switch-like formats give rise to larger heat fluxes transferred from the particle to the water, compared to sawtooth-like pulses. Consequently, more energy would be available from the water to drive bubble expansion when Q-switch-like pulse formats are employed, and larger bubbles would result. Another hypothesis is that the shielding effect produced by the cavitation bubbles (see section 4.5.1) might have a larger influence for the sawtooth-like format, compared to the Q-switch-like format. With the sawtooth-like shape, laser energy absorption would be shielded for the most intense part of the pulse. Conversely the

Biomedical Optics EXPRESS

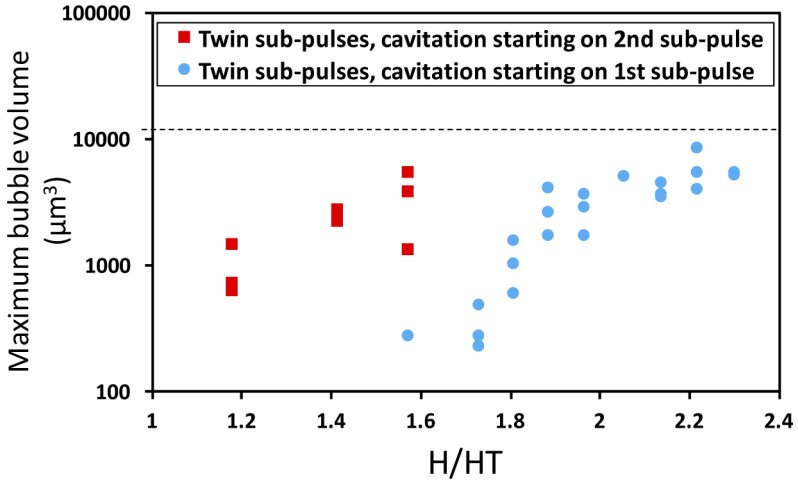

Fig. 11. Evolution of bubble volume with radiant exposure for melanin granules irradiated by two short (2.2 ns) identical consecutive sub-pulses separated by a delay of 630 ns. A reset of the bubble volume occurs at $H\sim 1.6\times H_T$, corresponding to the transition at which the cavitation starts to occur on the first sub-pulse.

Q-switch like shape this most intense part would not be shielded for a broad range of radiant exposures above threshold. With the Q-switch like format, the medium is irradiated upfront with the most intense part of the pulse, which would yield larger bubbles for the reasons just mentioned, whereas for the sawtooth-like format the shielding effect would "shut down" intense parts of the pulse that could otherwise produce larger temperature gradients and drive the growth of larger bubbles.

Another possible origin of the more explosive vaporizations observed with the Q-switch-like vs sawtooth-like pulses may be linked with the evolution of the bubble incipience time τ_{inc} at suprathreshold radiant exposures. As the radiant exposure is increased above threshold, the higher heating rates allow the nucleation temperature to be reached at earlier times, in other words τ_{inc} decreases with increasing radiant exposure. As such, τ_{inc} can be seen as an effective initial heating time or effective pulse duration for a given radiant exposure. The expanding bubble can thermally insulate the melanosome and to some extent potentially shield further absorption of laser energy at later times. Figure 12 shows the corresponding experimental data along with the thermal model's predictions for 630 ns long pulses. Clearly, $\tau_{inc\ (Q-switch)} < \tau_{inc\ (Sawtooth)}$ for a given relative radiant exposure. For example, at twice the threshold, $\tau_{inc\ (Q-switch)} \approx 133$ ns whereas $\tau_{inc\ (Sawtooth)} \approx 400$ ns.

A detailed model allowing the calculation of the relationship between the maximum bubble size and the laser pulse duration τ_p has been proposed by Faraggi et al.[7]. For rectangular pulses, the model predicts a significant decrease in the bubble size for $\tau_p > 100$ ns, which defines a typical "vaporization confinement time" τ_v. Reciprocally, the maximum bubble size is expected to grow as the heating time is reduced from a few hundreds of nanoseconds down to ≈100 ns or less. Considering this together with the data plotted in Fig. 12, an interpretation of the differences observed in the bubble size vs radiant exposure for Q-switch-like vs sawtooth-like formats can be postulated if one assumes that the maximum bubble size will start to increase significantly for radiant exposures where $\tau_{inc} \lesssim \tau_v$. The relative radiant exposure H_{RV} (normalized to threshold) for which $\tau_{inc} = \tau_v$, yields $H_{RV(Q-switch)} < H_{RV(Sawtooth)}$ from the results of Fig. 12. In other words, the radiant exposure above which significant increase of the maximum bubble size occurs is closer to the threshold for the Q-switch-like format than it is for the sawtooth format. This is

Biomedical Optics EXPRESS

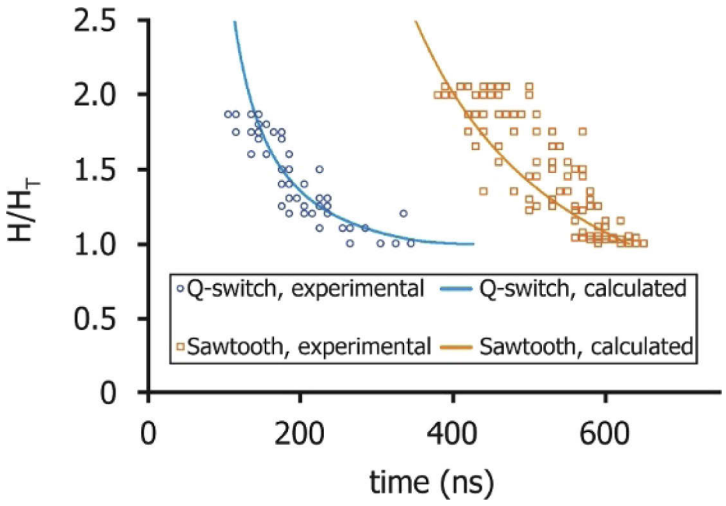

Fig. 12. Experimental vs calculated bubble incipience time (relative to the beginning of the pulse) for bovine melanosomes irradiated with Q-switch-like and sawtooth-like pulses of the same duration (630 ns), as a function of the radiant exposure (normalized with respect to the threshold exposure, vertical axis). At a given normalized radiant exposure, the onset of cavitation occurs at an earlier time for the Q-switch-like format, which is consistent with more explosive vaporizations observed with this pulse format, and given the model proposed by Faraggi et al. [7].

consistent with the result of Fig. 7B, where for the sawtooth format no significant increase of the bubble volume is observed between H_T and $2H_T$, as opposed to a steep increase starting at $1.4H_T$ with the Q-switch-like shape. The latter radiant exposure value can be employed to estimate τ_v from the thermal model fit shown in the left part of Fig. 12 (blue curve), since we assumed that the increase of the maximum bubble size starts at $\tau_{inc} \approx \tau_v$. For $H/H_T = 1.4$ the thermal model fit yields $\tau_{inc} = 190$ ns, which is within the order of magnitude predicted by Faraggi's model for the vaporization confinement time ($\tau_v \approx 100$ ns). Besides, extrapolation of the thermal model fit for the sawtooth-like shape (Fig. 12, orange curve) down to $\tau_{inc} = 190$ ns gives $H/H_T \approx 7$, which is consistent with the nearly constant bubble volume observed in the range of $H/H_T = 1 - 2$.

4.5.3. Self-limited growth of bubbles

The self-limited bubble growth reported by Neumann and Brinkmann [16] was not consistently observed in our experiments. Our results indicate that the inception of this type of bubble dynamics depends on the pulse shape being employed, not just pulse duration. Spatial effects could also be involved, as Neumann employed a top hat beam whereas our beam profile was Gaussian. Quantitative modeling of the influence of these factors on the onset of pulsational boiling within a spatial and temporal non-uniform temperature field may be complicated. However, the main consequence of our results is that the influence of the pulse shape cannot be ignored for controlling and optimizing the confinement of the thermal and bubble induced damage range and the safety range at a given radiant exposure. In this context, the sawtooth-like pulse format yielded the most consistent and predictable bubble sizes.

4.5.4. Bubble dynamics in the picosecond burst regime

As for the threshold, no difference in the bubble dynamics was found between the nanosecond and the picosecond burst regimes for radiant exposures up to $1.8H_T$. For $H = 1.8(180) = 324$ mJ/cm^2 and μ=12 000 cm^{-1} in melanosomes, the linearized model proposed by Sun and Gerstman

Biomedical Optics EXPRESS

[64] predict a peak stress of 667 kPa at the melanosome surface, which is four times higher than the saturated vapor pressure of water at a nucleation temperature of 387 K. The predicted tensile stress is ~40 kPa, using the same approach as in section 4.2. Nonetheless, compressive and tensile stresses resulting from thermoelastic expansion of the melanosome seem to have no impact on the vaporization kinetics and bubble growth for the bursts of picosecond pulses that were used in the experiments, which suggest that the thermoelastic stresses generated by the individual 60-ps sub-pulses were not strong enough to initiate a phase change. Different outcomes are expected with more energetic individual pulses, and possibly with bursts containing more energetic sub-pulses causing an increase of the Grüneisen coefficient during the burst, as discussed in section 4.2.

5. Conclusion

The influence of the pulse amplitude profile on bubble nucleation around microscopic melanin granules and melanosomes was investigated in the nanosecond and picosecond temporal pulse domains. For pulse duration longer than 50 ns, significant differences (up to 40%) in the threshold radiant exposures are observed, and at suprathreshold exposures the bubble dynamics are strongly influenced by the pulse shape. In particular, the onset of pulsating boiling leading to self-limited bubble growth was found to be pulse shape dependent. Our results demonstrate that pulse formats typically produced by Q-switch lasers are far from being optimized in terms of heat and bubble confinement. Sawtooth-like laser pulses with a positive slope yielded the most predictable bubble sizes around melanosomes, with a threshold typically 40% lower than Q-switch-like profiles. A thermal model accounting for local heating effects at the surface of melanin particles was developed and fitted with experimental cavitation energy thresholds. The fit allows for predicting the nucleation temperature and the μ of melanin, based on a statistical criterion involving the variance of the maximum temperature elevations calculated for the different pulse formats at threshold. For melanosomes, a μ=12 000 cm^{-1} was computed, which is higher than the value reported by Jacques et al. (2370 cm^{-1}) but close to the coefficients published by Brinkmann et al.[5]. The fits yielded nucleation temperatures of 387 ± 9 K and 388 ± 4 K for melanosomes and melanin granules, respectively. The bubble incipience time evolution with radiant exposure was studied and compared for the Q-switch-like and the sawtooth-like pulse formats. Fair agreement was obtained between the experimentally determined incipience times and the calculated ones. This data was further employed to interpret different bubble dynamics observed with these pulse shapes. Microcavitation experiments were also conducted with shaped bursts of picosecond pulses. The results suggest that in the tested irradiation conditions, thermoelastic stresses were not influencing the nucleation process, yielding cavitation thresholds and bubble dynamics similar to those found for nanosecond pulses having the same format and duration. The higher peak power of these bursts of picosecond pulses have the potential of improving the signal to noise ratio of photoacoustic dosimetry techniques for sub-microsecond laser eye surgeries and also increase the harmonic wavelengths conversion efficiencies in surgical lasers built around a near-infrared oscillator. Although not observed in our experiments, stress-confined bubble generation is thought possible in the picosecond burst regime for sub-pulse energy levels at least an order of magnitude higher than the level employed in this work, and would involve an increase of the Grüneisen coefficient during the burst. The use of single picosecond pulses instead of bursts could also be considered as stress-confined bubble generation with lower thresholds has been demonstrated, at least for homogeneous nucleation [20,36,36]. However, Kelly [11] and Payne [19] found similar cavitation thresholds in the ns vs fs-ps regimes for melanosome suspensions and RPE cells. Besides, shorter pulses tend to produce steeper increases of the bubble size with radiant exposure, which can limit the therapeutic range for retinal surgical procedures. Shorter pulses can also be affected (shape, duration, beam profile) by group velocity dispersion and non-linear effects when propagating in a delivery optical fiber and in the eye itself,

Biomedical Optics EXPRESS

and are generally produced at a higher cost per photon. Based on the results of this study, we conclude that pulses with sawtooth shapes and durations of a few hundreds of nanoseconds could represent the optimal pulse parameters for SRT. In this regime, the bubble size can be kept almost constant for radiant exposures up to twice the cavitation threshold, with a threefold reduction in the threshold (when employing 630 ns-pulses) compared to the typical pulse parameters currently used in SRT. These pulse formats can be easily and reliably delivered via optical fiber coupling, without pulse distortion. Such sawtooth shapes can be achieved, at least in principle, with relatively compact, low cost, customized and frequency-doubled Q-switch lasers. At a higher cost per photon, more sophisticated, frequency-doubled fiber lasers can offer a finer control over the pulse shape with the added benefit of producing sawtooth-shaped bursts of ps pulses for improved photoacoustic dosimetry during the surgical procedures. Altogether, these outcomes demonstrate that sub-microsecond pulse shaping may provide an efficient means of controlling laser-directed microcavitation in numerous applications requiring optimized thermal and mechanical damage confinement, including highly selective cell targeting in retinal therapies.

Funding

Canadian Institutes of Health Research.

Acknowledgments

The authors want to thank Yves Taillon from INO for providing a programmable MOPAW laser system that was used for the microcavitation experiments. We also thank Frédéric Émond for his invaluable help in assembling the pump probe setup and conducting the experiments.

Disclosures

The authors declare that there are no conflicts of interest related to this article.

References

1. C. Alt Detection of Intracellular Cavitation During Selective Targeting of the Retinal Pigment Epithelium With a Laser Scanner [Ph.D. thesis]. 2008.
2. C. Alt, C.M. Pitsillides, J. Roegener, and C.P. Lin, "Monitoring Intracellular Cavitation During Selective Targeting of the Retinal Pigment Epithelium," Proc. SPIE **4951**, 48–55 (2003).
3. R. Brinkmann, J. Roider, and R. Birngruber, "Selective retina therapy (SRT): a review on methods, techniques, preclinical and first clinical results," Bull. Soc. Belge Ophtalmol. **302**, 51–69 (2006).
4. R. Brinkmann and R. Birngruber, "Selektive Retina-Therapie (SRT)," Z. Med. Phys. **17**(1), 6–22 (2007).
5. R. Brinkmann, G. Hüttmann, J. Rögener, J. Roider, R. Birngruber, and C.P. Lin, "Origin of retinal pigment epithelium cell damage by pulsed laser irradiance in the nanosecond to microsecond time regimen," Lasers Surg. Med. **27**(5), 451–464 (2000).
6. F. Fankhauser and S. Kwasniewska, *Lasers in Ophthalmology: Basic, Diagnostic, and Surgical Aspects: A Review*. (Kugler Publications, ed.).; 2003.
7. E. Faraggi, B.S. Gerstman, and J. Sun, "Biophysical effects of pulsed lasers in the retina and other tissues containing strongly absorbing particles: shockwave and explosive bubble generation," J. Biomed. Opt. **10**(6), 064029 (2005).
8. C. Framme, A. Walter, P. Prahs, D. Theisen-Kunde, and R. Brinkmann, "Comparison of threshold irradiances and online dosimetry for selective retina treatment (SRT) in patients treated with 200 nanoseconds and 1.7 microseconds laser pulses," Lasers Surg. Med. **40**(9), 616–624 (2008).
9. B.S. Gerstman, C.R. Thompson, S.L. Jacques, and M.E. Rogers, "Laser induced bubble formation in the retina," Lasers Surg. Med. **18**(1), 10–21 (1996).
10. M.W. Kelly and C.P. Lin, "Microcavitation and cell injury in RPE cells following short-pulsed laser irradiation," Proc. SPIE **2975**, 174–179 (1997).
11. M.W. Kelly Intracellular cavitation as a mechanism of short-pulse laser injury to the retinal pigment epithelium [Ph.D. thesis]. 1997.
12. H. Lee, C. Alt, C.M. Pitsillides, and C.P. Lin, "Optical detection of intracellular cavitation during selective laser targeting of the retinal pigment epithelium: dependence of cell death mechanism on pulse duration," J. Biomed. Opt. **12**(6), 064034 (2007).
13. C.P. Lin and M.W. Kelly, "Cavitation and acoustic emission around laser-heated microparticles," Appl. Phys. Lett. **72**(22), 2800–2802 (1998).

Biomedical Optics EXPRESS

14. C.P. Lin, M.W. Kelly, S.A.B. Sibayan, M.A. Latina, and R.R. Anderson, "Selective cell killing by microparticle absorption of pulsed laser radiation," IEEE J. Sel. Top. Quantum Electron. **5**(4), 963–968 (1999).
15. J. Neumann and R. Brinkmann, "Boiling nucleation on melanosomes and microbeads transiently heated by nanosecond and microsecond laser pulses," J. Biomed. Opt. **10**(2), 024001 (2005).
16. J. Neumann and R. Brinkmann, "Self-limited growth of laser-induced vapor bubbles around single microabsorbers," Appl. Phys. Lett. **93**(3), 033901 (2008).
17. J. Neumann, R. Brinkmann, M. Laserzentrum, L. Gmbh, and D. Lübeck, "Microbubble dynamics around laser heated microparticles," Proc. SPIE **5142**, 82–87 (2003).
18. Y.G. Park, E. Seifert, Y.J. Roh, D. Theisen-Kunde, S. Kang, and R. Brinkmann, "Tissue response of selective retina therapy by means of a feedback-controlled energy ramping mode," Clin Experiment Ophthalmol **42**(9), 846–855 (2014).
19. D.J. Payne, T.R. Jost, J.J. Elliot, B. Eilert, L. Lott, K. Lott, G.D. Noojin, R.A. Hopkins Jr., C.P. Lin, and B.A. Rockwell, "Cavitation thresholds in the rabbit retina pigmented epithelium," Proc. SPIE **3601**, 27–31 (1999).
20. B.A. Rockwell, R.J. Thomas, and A. Vogel, "Ultrashort laser pulse retinal damage mechanisms and their impact on thresholds," Med Laser Appl. **25**(2), 84–92 (2010).
21. J. Roegener, R. Brinkmann, and C.P. Lin, "Pump-probe detection of laser-induced microbubble formation in retinal pigment epithelium cells," J. Biomed. Opt. **9**(2), 367–371 (2004).
22. J. Roider, R. Brinkmann, and R. Birngruber, "Selective retinal pigment epithelium laser treatment," In: F. Fankhauser and S. Kwasniewska, eds. *Lasers in Ophthalmology: Basic, Diagnostic, and Surgical Aspects: A Review*. ; 2003.
23. J. Roider, F. Hillenkamp, T. Flotte, and R. Birnnguber, "Microphotocoagulation: Selective effects of repetitive short laser pulses," Proc. Natl. Acad. Sci. U. S. A. **90**(18), 8643–8647 (1993).
24. P. Steiner, A. Ebneter, L.E. Berger, M. Zinkernagel, B. Považay, C. Meier, J.H. Kowal, C. Framme, R. Brinkmann, S. Wolf, and R. Sznitman, "Time-resolved ultra-high resolution optical coherence tomography for real-time monitoring of selective Retina therapy," Invest. Ophthalmol. Visual Sci. **56**(11), 6654–6662 (2015).
25. H. Stoehr, L. Ptaszynski, A. Fritz, and R. Brinkmann, "Interferometric Optical Online Dosimetry for Selective Retina Treatment (SRT)," Proc. SPIE **6632**, 663219 (2007).
26. J.P.M. Wood, M. Plunkett, V. Previn, G. Chidlow, and R.J. Casson, "Nanosecond pulse lasers for retinal applications," Lasers Surg. Med. **43**(6), 499–510 (2011).
27. E. Boulais, R. Lachaine, A. Hatef, and M. Meunier, "Plasmonics for pulsed-laser cell nanosurgery: Fundamentals and applications," J. Photochem. Photobiol., C **17**, 26–49 (2013).
28. Y. Zhou, X.-Y. Zhou, Z.-G. Wang, Y.-F. Zhu, and P. Li, "Elevation of plasma membrane permeability upon laser irradiation of extracellular microbubbles," Lasers Surg. Med. **25**(4), 587–594 (2010).
29. A. Vogel and V. Venugopalan, "Mechanisms of Pulsed Laser Ablation of Biological Tissues," Chem. Rev. **103**(2), 577–644 (2003).
30. M. Niemz, *Laser-Tissue Interactions -Fundamentals and Applications*. 3rd ed. Springer, New York; 2007.
31. A. Vogel and V. Venugopalan, "Pulsed laser ablation of soft biological tissues," In: *Optical-Thermal Response of Laser-Irradiated Tissue*. 2nd ed. Springer, New York; 2011.
32. D.M. Simanovskii, M.A. Mackanos, A.R. Irani, C.E. O'Connell-Rodwell, C.H. Contag, H.A. Schwettman, and D.V. Palanker, "Cellular tolerance to pulsed hyperthermia," Phys. Rev. E **74**(1), 011915 (2006).
33. S. Thomsen and J.A. Pearce, "Thermal Damage and Rate Processes in Biologic Tissues," In: *Optical-Thermal Response of Laser-Irradiated Tissue*. 2nd ed. Springer, New York; 2011.
34. A. Vogel Optical Breakdown in Water and Ocular Media and Its Use for Intraocular Photodisruption. Habilitation dissertation, Aachen: Shaker; 2001.
35. A. Vogel, J. Noack, G. Hüttmann, and G. Paltauf, "Mechanisms of femtosecond laser nano surgery of biological cells and tissues," Appl. Phys. B **81**(8), 1015–1047 (2005).
36. A. Vogel, N. Linz, S. Freidank, and G. Paltauf, "Femtosecond laser induced nanocavitation in water: implications for optical breakdown threshold and cell surgery," Phys. Rev. Lett. **100**(3), 038102 (2008).
37. G. Paltauf and P.E. Dyer, "Photomechanical processes and effects in ablation," Chem. Rev. **103**(2), 487–518 (2003).
38. J.H. Lock and K.C.S. Fong, "Retinal laser photocoagulation," Retina **19**(3), 193–198 (1989).
39. C. Sramek, L.S. Leung, T. Leng, J. Brown, Y.M. Paulus, G. Schuele, and D. Palanker, "Improving the therapeutic window of retinal photocoagulation by spatial and temporal modulation of the laser beam," J. Biomed. Opt. **16**(2), 028004 (2011).
40. J. Marshall, A. M. Hamilton, and A. C. Bird, "Histopathology of ruby and argon laser lesions in monkey and human retina. A comparative study," Br. J. Ophthalmol. **59**(11), 610–630 (1975).
41. J. Roider, N.A. Michaud, T.J. Flotte, and R. Birngruber, "Response of the retinal pigment epithelium to selective photocoagulation," Arch. Ophthalmol. **110**(12), 1786–1792 (1992).
42. C.P. Lin and M.W. Kelly, "Ultrafast time-resolved imaging of stress transient and cavitation from short pulsed laser irradiated melanin particles," Proc. SPIE **2391**, 294–299 (1995).
43. R. Brinkmann, J. Roegener, C.P. Lin, J. Roider, R. Birngruber, and G. Huettmann, "Selective RPE photodestruction: mechanism of cell damage by pulsed-laser irradiance in the ns to µs time regime," Proc. SPIE **3601**, 59–65 (1999).
44. C. Framme, G. Schuele, J. Roider, R. Birngruber, and R. Brinkmann, "Influence of Pulse Duration and Pulse Number in Selective RPE Laser Treatment," Lasers Surg. Med. **34**(3), 206–215 (2004).

Biomedical Optics EXPRESS

45. C. Framme, G. Schuele, J. Roider, D. Kracht, R. Birngruber, and R. Brinkmann, "Threshold determinations for selective retinal pigment epithelium damage with repetitive pulsed microsecond laser systems in rabbits," Ophthalmic Surg. Lasers **33**(5), 400–409 (2002).
46. C. Framme, G. Schuele, K. Kobuch, B. Flucke, R. Birngruber, and R. Brinkmann, "Investigation of selective retina treatment (SRT) by means of 8 ns laser pulses in a rabbit model," Lasers Surg. Med. **40**(1), 20–27 (2008).
47. S.L. Jacques, "Role of tissue optics and pulse duration on tissue effects during high-power laser irradiation," Appl. Opt. **32**(13), 2447–2454 (1993).
48. L. Zhigilei and B. Garrison, "Microscopic simulation of short pulse laser damage of melanin particles," Proc. SPIE **3254**, 135–143 (1998).
49. D.D.M. Ho, R. London, G.B. Zimmerman, and D.A. Young, "Laser-tattoo removal—A study of the mechanism and the optimal treatment strategy via computer simulations," Lasers Surg. Med. **30**(5), 389–397 (2002).
50. J.J. Weiter, F.C. Delori, G.L. Wing, and K.A. Fitch, "Retinal pigment epithelial lipofuscin and melanin and choroidal melanin in human eyes," Investig Ophthalmol Vis. Sci. **27**(2), 145–152 (1986).
51. I.T. Kim and J.B. Choi, "Melanosomes of retinal pigment epithelium–distribution, shape, and acid phosphatase activity," Korean J. Ophthalmol. **12**(2), 85–91 (1998).
52. X. Peng, B. Baird, W. Ren, D. Hemenway, L. Xu, P. Deladurantaye, Y. Taillon, M. Frede, and D. Kracht, "355 nm Tailored Pulse Tandem Amplifier," *Adv Solid-State Photonics.* 2008:MC35.
53. P. Deladurantaye, M. Drolet, L. Desbiens, Y. Taillon, B. Labranche, V. Roy, and P. Laperle, "140-μJ, narrow-linewidth, robustly single-transverse mode nanosecond infrared fiber laser platform with fine pulse tailoring capability," Proc. SPIE **7386**, 73860Q (2009).
54. P. Deladurantaye, V. Roy, L. Desbiens, M. Drolet, Y. Taillon, and P. Galarneau, "Ultra Stable, Industrial Green Tailored Pulse Fiber Laser with Diffraction-limited Beam Quality for Advanced Micromachining," J. Phys.: Conf. Ser. **276**, 012017 (2011).
55. P. Deladurantaye, A. Cournoyer, M. Drolet, L. Desbiens, D. Lemieux, M. Briand, and Y. Taillon, "Material micromachining using bursts of high repetition rate picosecond pulses from a fiber laser source," Proc. SPIE**7914**, 791404 (2011).PSISDG0277-786X
56. P. Deladurantaye, L. Desbiens, V. Roy, and Y. Taillon Device and method for generating bursts of picosecond optical sub-pulses [US Patent 8,798,107]. 2014.
57. L. Desbiens, M. Drolet, V. Roy, M.M. Sisto, and Y. Taillon, "Arbitrarily-shaped bursts of picosecond pulses from a fiber laser source for high-throughput applications," Proc. SPIE **7914**, 791420 (2011).
58. H. Goldenberg and C.J. Tranter, "Heat flow in an infinite medium heated by a sphere," Br. J. Appl. Phys. **3**(9), 296–298 (1952).
59. J. Neumann and R. Brinkmann, "Nucleation dynamics around single microabsorbers in water heated by nanosecond laser irradiation," J. Appl. Phys. **101**(11), 114701 (2007).
60. S.L. Jacques, R.D. Glickman, and J.A. Schwartz, "Internal absorption coefficient and threshold for pulsed laser disruption," Proc. SPIE **2681**, 468–477 (1996).
61. S.L. Jacques and D.J. McAuliffe, "The melanosome: threshold temperature for explosive vaporization and internal absorption coefficient during pulsed laser irradiation," Photochem. Photobiol. **53**(6), 769–775 (1991).
62. I. Vitkin and J. Woolsey, "Optical and thermal characterization of natural (Sepia officinalis) melanin," Photochem. Photobiol. **59**(4), 455–462 (1994).
63. J.E. De Albuquerque, C. Giacomantonio, A.G. White, and P. Meredith, "Determination of thermal and optical parameters of melanins by photopyroelectric spectroscopy," Appl. Phys. Lett. **87**(6), 061920 (2005).
64. J. Sun and B.S. Gerstman, "Pressure generation in melanosomes by subnanosecond laser pulses," Proc. SPIE **3254**, 156–167 (1998).
65. S.L. Jacques, A.A. Oraevsky, C.R. Thompson, and B.S. Gerstman, "Working theory and experiments on photomechanical disruption of melanosomes to explain the threshold for minimal visible retinal lesions for sub-ns laser pulses," Proc. SPIE **2134**, 8 (1994).
66. M. Strauss, P.A. Amendt, R.A. London, D.J. Maitland, M.E. Glinsky, C.P. Lin, and M.W. Kelly, "Computational modeling of stress transient and bubble evolution in short-pulse laser-irradiated melanosome particles," Proc. SPIE **2975**, 261–270 (1997).